ORIGINAL PAPER

Variation of reaction dynamics for OH hydrogen abstraction from glycine between *ab initio* levels of theory

Ren-Jie Lin · Chen-Chang Wu · Soonmin Jang · Feng-Yin Li

Abstract The variation in reaction dynamics of OH hydrogen abstraction from glycine between HF, MP2, CCSD(T), M05-2X, BHandHLYP, and B3LYP levels was demonstrated. The abstraction mode shows distinct patterns between these five levels and determines the barrier height, and the spin density transfer between OH radical and glycine. These differences are mainly resulted from the spin density distribution and geometry of the alpha carbon during the abstraction. The captodative effect which is commonly believed as one of the major factors to stabilize the caron-centered radical can only be observed in DFT levels but not in HF and MP2 levels. Difference in the abstraction energy were found in these calculation levels, by using the result of CCSD(T) as reference, B3LYP, BHandHLYP, and M05-2X underestimate the reaction barrier about 5.1, 0.1, and 2.4 kcal mol^{-1}, while HF and MP2 overestimated 19.1 kcal mol^{-1} and 1.6 kcal mol^{-1}, respectively. These differences can be characterized by the vibration mode of imaginary frequency of transition states, which indicates the topology around transition states and determines reaction barrier height. In this model system, BHandHLYP provides the best prediction of the energy barrier among those tested methods.

R.-J. Lin · C.-C. Wu · F.-Y. Li (✉)
Department of Chemistry, National Chung Hsing University,
Taichung,
402 Taiwan, Republic of China
e-mail: feng64@nchu.edu.tw

S. Jang
Department of Chemistry, Sejong University,
Seoul 143-747, Korea

Introduction

In order to obtain reliable reaction mechanisms, various levels of theory ranging from basic Hartree–Fock (HF) theory, through post-HF theory, such as *n*th order Møller-Plesset (MPn), and density functional theory (DFT), to high-level methods including coupled cluster theory (CCT) like CCSD(T), are commonly used and expected to generate accurate results proportional to the level of sophistication. One of the major advantages of DFT is its computational efficiency as compared to conventional correlation methods (MPn and CCT). The accuracy of DFT applying gradient-corrected functionals is about the same as that of MP2. [1-4] Nowadays the molecular species with size relevant for both academic and industrial chemists are implemented almost exclusively with DFT calculations. However, in some cases, some DFT methods, such as B3LYP [5, 6], tend to underestimate the reaction barriers, while MP2 overestimates them, especially reactions involving hydrogen atoms[6, 7]. So far it has been attributed to the poor description of the long-range electron correlation in conventional exchange functionals such as B3LYP[6, 7]. Although there are extensive studies on the long-range exchange effects in DFT, including systematical parameterization against various reaction databases [8-11], to our knowledge, there are no studies concerning the variation in reaction dynamics along with the reaction pathway, explained by electronic properties such as spin density and charge distribution, due to the calculation levels. In this study, we investigated this variation by detailing the potential energy surface (PES) along the reaction pathway,

Fig. 1 The geometries of TS complexes at B3LYP level for the N-terminal channel (a) and the C-terminal channel (b)
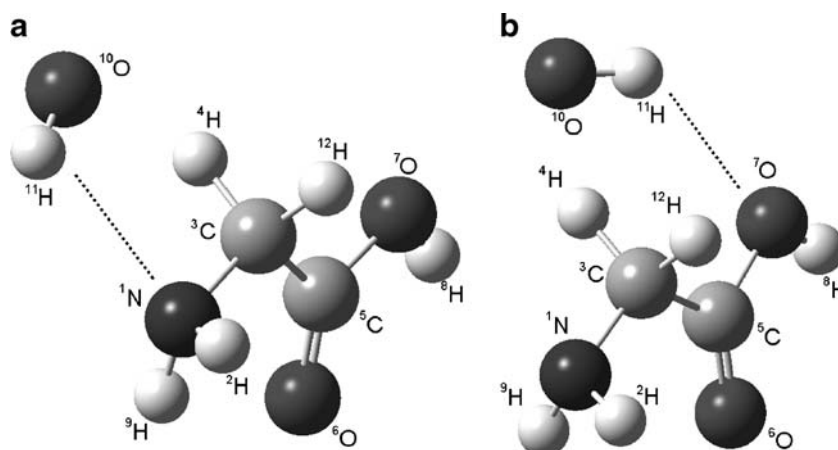

which can be characterized by performing the intrinsic reaction coordinate (IRC) analysis [12-14] and provide an explanation of the consequence between the different *ab initio* methods in terms of the molecular and electronic structures. IRC is a static analysis of a one-dimensional cut through a PES related to a specific reaction and can provide a convenient starting point for the reaction dynamics. Defined as the steepest descent path, the minimum energy path (MEP) connects a reactant minimum, a product minimum and their related transition state (TS) or first-order saddle point on the PES verified through IRC calculation. Knowledge of the MEP and the related energies, gradients and second derivatives (hessians) facilitates the determination of the associated reaction mechanism. Through this study, we intended to provide new insight in the reaction barrier heights, especially in hydrogen transfer reactions when calculated with *ab initio* calculations. It can also resolve the issue why the pre-reactive complexes of certain hydrogen abstraction reactions are very elusive when calculated at DFT levels, especially at B3LYB level [15, 16].

Computation methods

We used OH hydrogen abstraction from glycine as an example to demonstrate the variation in MEP due to different calculation methods. As the simplest amino acid, glycine has been used as a model system for protein reactions [17-19]. Furthermore, a detailed study of this OH hydrogen abstraction reaction at various calculation levels was available in literature [20]. We used B3LYP, BHandH-LYP, M05-2X, Hartree-Fock (HF) and MP2 methods with the standard basis set 6-311++G**, which involves double diffusion and polarization functions, compared with M05-2X developed recently by Truhlar *et al*. [21]. The geometries of the reactants, transition states, pre-reactive complexes, and post-reactive complexes were obtained by full optimization and checked with frequency calculations. Furthermore, IRC calculations were performed to verify a particular TS connecting to its related pre-reactive and post-reactive complexes. Zero-point energies were included in the determination of the reaction heat and activation

Fig. 2 Energy profile of two reaction channel for OH hydrogen abstraction from glycine in the B3LYP level with ZPE. The energy unit is in kcal mol^{-1} and bond-length is in Å
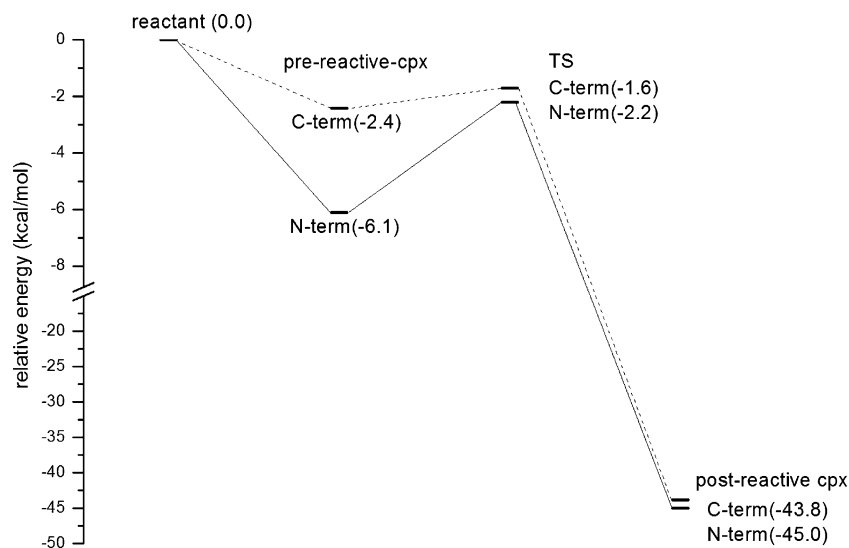
Table 1 Comparison of transition state characteristics for C-terminal channel between various calculation methods

Level	Bond length (Å)				Bond angle (°)	
	^{11}H-^{10}O	^{10}O-^{4}H	^{3}C-^{4}H	^{7}O-^{11}H	^{4}H-^{10}O-^{11}H	^{10}O-^{4}H-^{3}C
B3LYP	0.976	1.838	1.117	2.331	94.1	150.9
M05-2X	0.969	1.514	1.155	2.374	96.7	159.1
BHandHLYP	0.960	1.423	1.177	2.634	98.1	168.5
MP2	0.970	1.374	1.180	2.534	96.1	166.6
HF	0.949	1.264	1.268	2.888	99.4	175.3

*The number labeling is the same as Fig. 1 and all methods are with 6-311++G** basis set

energies. Conductor-like polarizable continuum model (CPCM) was used to simulate the reaction in aqueous environment. The United Atom model for Hartree-Fock (UAHF) definition [22] was employed for the construction of the solute cavity. All calculations were performed by Gaussian03 program [23]. Since the OH hydrogen abstraction involves the bonding of the C_α switching from sp^3 to sp^2 hybridization, the analysis methods were designed to monitor this hybridization change including the geometry, energetics and spin density along the MEP.

Results and discussion

There are two channels in the H_α abstraction reaction of glycine as shown in Fig. 1 obtained at BHandHLYP level. One is the C-terminal channel with the OH radical forming hydrogen bond with the hydroxyl group of glycine, and the other is the N-terminal one with the hydrogen bond formed with the amino group. Their energy profiles were shown in Fig. 2. The N-terminal pre-reactive complex is more stable than the C-terminal one but its related energy barrier is 3.2 kcal mol^{-1} higher than that found in the C-terminal one. However, the energy differences between the transition

states and post-reactive complexes for these two channels are only 0.6 and 1.2 kcal mol^{-1}, respectively. Therefore, the N-terminal channel can be considered as a thermodynamic favorite while the C-terminal channel is a kinetic favorite. The product generated from the C-terminal channel should be the major product. However, there is a rotational transformation between the N- and C-terminal complexes with a small energy barrier. In the following, we used the C-terminal channel to demonstrate the reaction mechanism of this OH hydrogen abstraction from glycine. A comparison between these five different methods for the TS was shown in Tables 1 and 2. The TS geometries are similar between these calculation methods except for the distance between the oxygen of the OH radical and H_α, i.e., ^{10}O-^{4}H. However, the TS imaginary frequency is quite sensitive between these methods, and the longer the ^{10}O-^{4}H, the smaller the absolute value of the imaginary frequency. The imaginary frequency varies, for example, there is more than one order of magnitude difference between MP2 and B3LYP. As shown in Table 2, the barrier height with B3LYP, M05-2X, BHandHLYP, MP2, and HF are 0.8, 3.5, 5.8, 7.5, and 25.0 kcal mol^{-1}, respectively. Their corresponding imaginary frequencies are -112.3, -852.4, -903.2, -1537.1, and -3136.7 cm^{-1}, respectively. The results

**Table 2** The relationship between the TS imaginary frequency, energy barrier and reaction heat

Level	Imaginary freq. (cm^{-1})	Barrier (kcal/mol)	ΔH (kcal/mol)	CPCM (water)	
				Barrier (kcal/mol)	ΔH (kcal/mol)
B3LYP	-112.29	1.3/0.8	-41.5/-41.3	-	-
M05-2X	-852.35	5.9/3.5	-41.3/-40.9	5.4	-40.2
BHandHLYP	-903.21	8.6/5.8	-34.1/-34.4	8.8	-33.6
MP2	-1537.14	10.6/7.5	-38.6/-38.3	-	-
HF	-3136.71	27.4/25.0	-19.8/-19.9	-	-
CCSD(T)^b	N.A.	5.9	-35.7	-	-
CCSD(T)^c	N.A.	6.6	-35.1	-	-
CCSD(T)^d	N.A.	6.7	-35.6	-	-

^{a} Barrier (the value without ZPE/ with ZPE) and all methods are with 6-311++G** basis set

^{b} CCSD(T)/6-311++G(2d,p)//BHandHLYP/6-311++G**

^{c} CCSD(T)/6-311++G(2d,p)//M05-2X/6-311++G**

^{d} CCSD(T)/6-311++G(2d,p)//MP2/6-311++G**
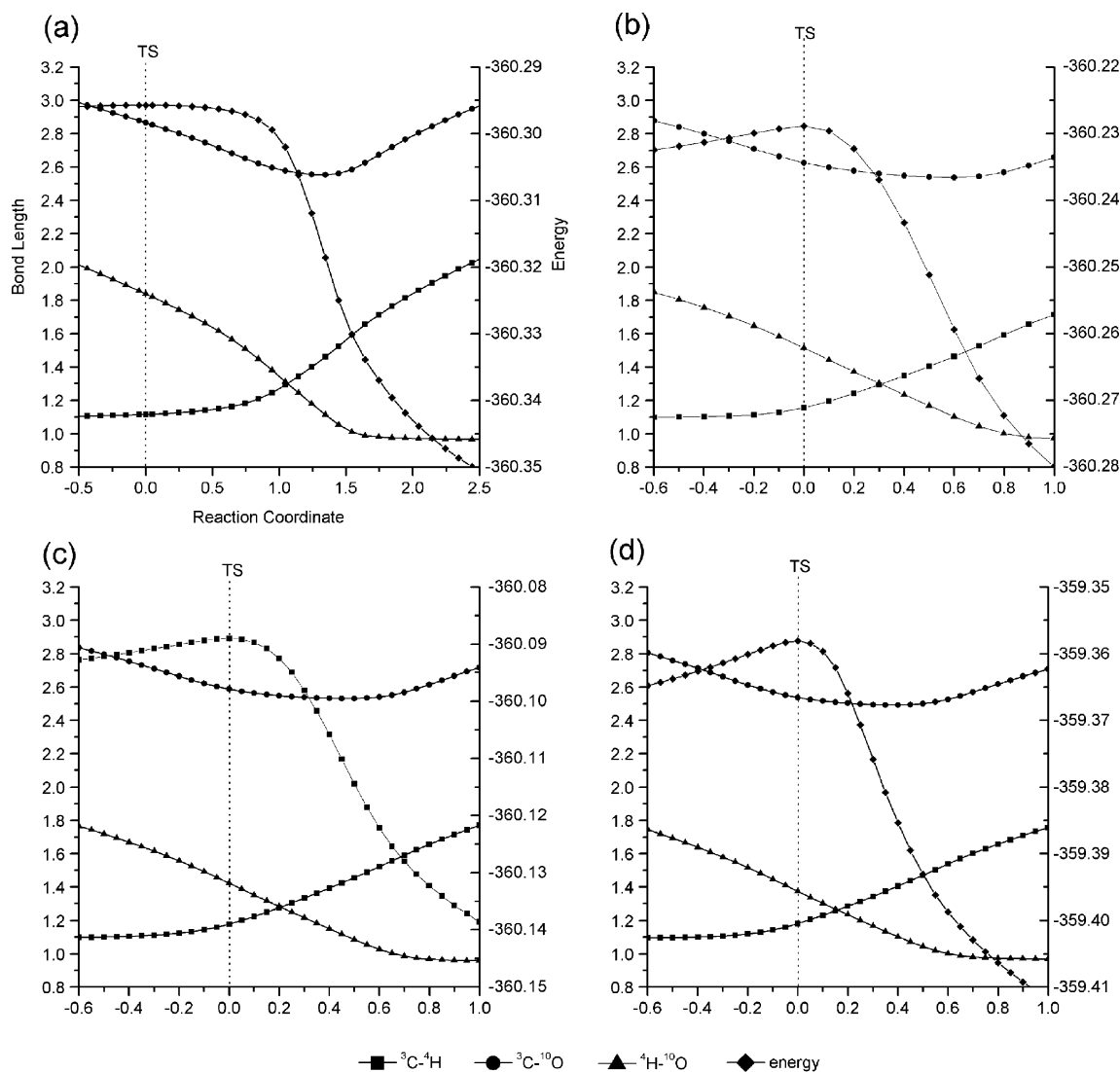
Fig. 3 Energies and several relevant bond-lengths of the conformations along the reaction pathway. Methods used from top to bottom are (**a**) B3LYP, (**b**) M05-2X, (**c**) BHandHLYP, and (**d**) MP2 levels,

respectively. All symbols in Fig. 3(**b**), (**c**), and (**d**) are the same as Fig. 3(**a**). The units in bond length and energy are Å, and Hartree, respectively

indicate that larger barrier height is associated with more negative imaginary frequency. Our results are consistent with those found by Galano *et al.* [20]. Similar phenomena were also reported by Zhao *et al.* [6] on the MUE (mean unsigned error) of barrier height for hydrogen transfer reactions in a benchmark database with various calculation levels. In this study, we reported an integral view regarding to the difference in the barrier height, the TS imaginary frequency and MEP caused by the five calculation levels through the analyses of the geometries, energetics and spin densities of the structures along the reaction pathway obtained by IRC calculation.

As shown in Fig. 3, the abstraction process of H_α at TS varies among the methods used. To facilitate the discussion, we defined the starting point of the abstraction process as when the H_α lies halfway between the hydroxyl oxygen and

the C_α, i.e., the crossing point between the $C_\alpha - H_\alpha$ and $O_{radical}-H_\alpha$ lines in Fig. 3. This abstraction started at 1.044, 0.299, 0.199, 0.149, and 0.000 s(amu)$^{1/2}$ Bohr along the forward path away from the TS at the B3LYP, M05-2X, BHandHLYP, MP2 and HF (the data of HF level are not shown for simplicity) levels, respectively. Therefore the TS obtained at the MP2, M05-2X, BHandHLYP and B3LYP levels can be considered as reactant-like since the breakage of C_α-H_α bond occurs later than the TS, but at the HF level, the abstraction started right at the TS. The energy barrier becomes smaller as the delay between the abstraction point and the TS increases. Based on our results, the calculation methods can be characterized according to the delay of the abstraction from the TS, i.e., B3LYP in one end of the spectrum and HF in the other end with MP2 close to the HF end and BHandHLYP close to the B3LYP end. As shown in

Fig. 4 Atomic spin density of glycine along the reaction pathway. The order of the calculation methods is the same as in Fig. 3
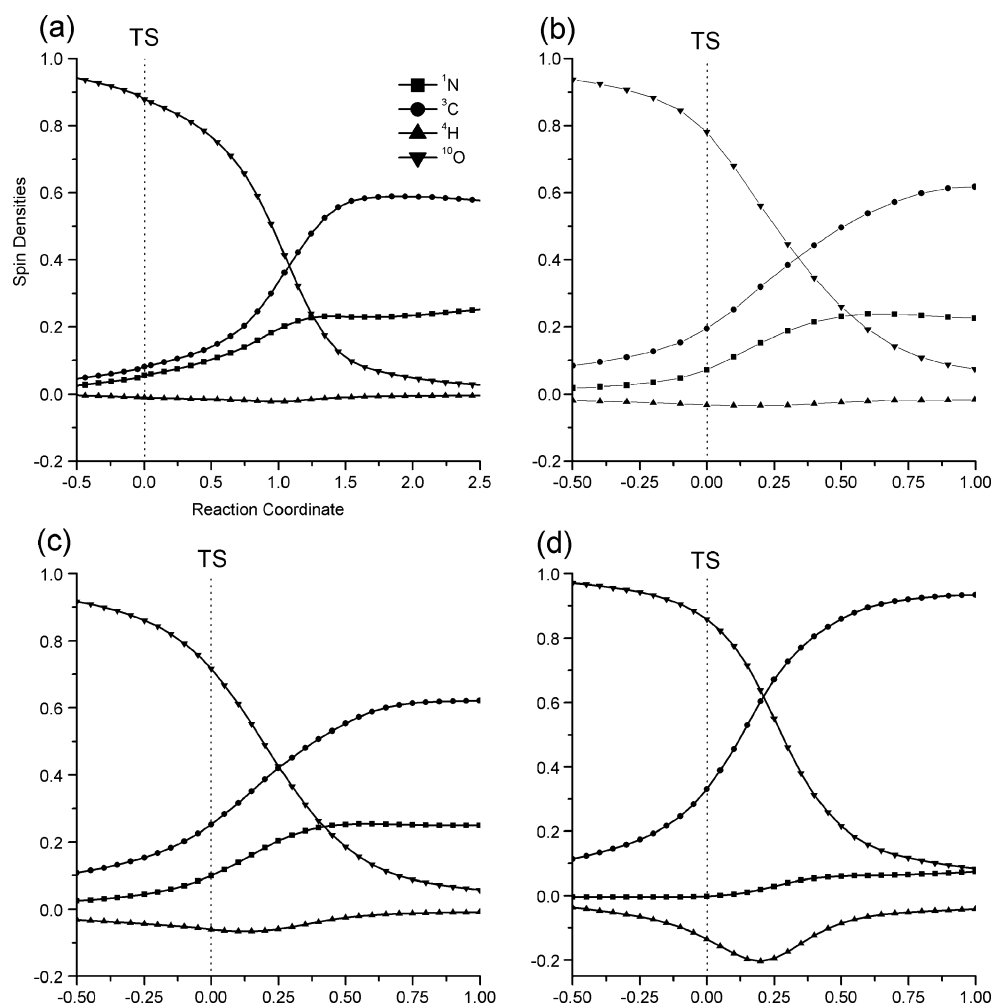

Table 2, we also used those optimized structures obtained by BHandHLYP, M05-2X, and MP2 levels to perform single point calculations with CCSD(T) level. The energy barrier with CCSD(T) single point calculations are 5.9, 6.6, and 6.7 kcal mol^{-1}, respectively. We also performed the CPCM calculations to realize reaction barrier in aqueous environment with BHandHLYP and M05-2X levels which can provide accurate barrier height. Interestingly the barrier height in water is about 2 kcal mol^{-1} higher than that in gas phase. The correlation between the energy barrier and the delay of the abstraction from the TS can be explained by the imaginary vibration mode of the TS obtained by the methods used. (The motion pictures of this vibration mode at these five levels were provided in supplementary materials.) At the HF level, the TS imaginary vibration mode is dominated by a simple oscillation of the H_α between the hydroxyl oxygen atom and C_α, while this vibration mode at the B3LYP level is more like a rocking motion between OH radical to glycine with the length of the C_α-H_α bond almost fixed. The TS imaginary vibration mode at the MP2 level is similar to that at the HF level but involves some rocking motion similar to that found in

B3LYP. The portion of this rocking motion increases in the TS imaginary vibration mode at the M05-2X and BHandH-LYP levels compared to the MP2 level. The different motion of the TS imaginary vibration mode between the calculation methods, i.e., the bond stretching and rocking motion, results in an imaginary frequency more than one order of magnitude difference between HF and B3LYP. This difference in the TS imaginary vibration mode also causes the variation in MEP and provides an explanation for the difference in barrier height calculated between the five calculation methods. The characterization of the variation in this reaction dynamics caused by the different calculation methods can be reduced to the distance between the hydroxyl oxygen and C_α along the reaction path. In one extreme found in B3LYP, the OH radical approaches the C_α with a total energy and C_α-H_α bond-length remaining roughly the same until the H_α reaches the abstraction point through rocking motion of the side chain and NH_2 group. At the HF level, the distance between the hydroxyl oxygen and the C_α atom remains 2.52Å during the reaction coordinate from 0.0 to 0.399 s(amu)$^{1/2}$ Bohr while the H_α approaches the hydroxyl oxygen. This indicates that the

Table 3 The spin density at several important points along the reaction pathway

Level	$^{\$}$PRC	N	C_α	H_α	$O_{radical}$
B3LYP	TS	0.054	0.081	-0.010	0.879
	ABS	0.202	0.361	-0.021	0.414
	PV	0.251	0.577	-0.004	0.027
M05-2X	TS	0.071	0.194	-0.032	0.781
	ABS	0.188	0.384	-0.032	0.447
	PV	0.226	0.618	-0.016	0.074
BHandHLYP	TS	0.099	0.252	-0.060	0.716
	ABS	0.183	0.386	-0.064	0.489
	PV	0.249	0.621	-0.009	0.058
MP2	TS	-0.001	0.331	-0.135	0.858
	ABS	0.011	0.529	-0.197	0.715
	PV	0.074	0.934	-0.042	0.083
HF	TS	0.056	0.540	-0.210	0.668
	ABS	0.056	0.540	-0.210	0.668
	PV	0.124	0.899	-0.024	0.050

$^{\$}$ PRC is the point of the reaction coordinate; TS is the transition state; ABS is the abstraction point and PV is the plateau value; All methods are with 6-311++G** basis set

reaction channel goes mostly through the bond stretching of the C_α-H_α bond at TS. This explains why the barrier height at the B3LYP level is low since TS involves more rocking motion compared to that found in other methods used and therefore the energy landscape around the TS is relatively flat. The barrier height at the HF level is over-estimated and MEP around TS declines more steeply than that at the B3LYP level. According to the pattern found in the distance of the hydroxyl oxygen and C_α, M05-2X is close to B3LYP and MP2 is close to HF, similarly with the order found with the TS imaginary vibration mode. Interestingly, these patterns found in BHandHLYP lie between those found in M05-2X and MP2. From the above analysis, the main reason for the elusive pre-reactive complexes of OH hydrogen abstraction reactions in peptides or proteins when

calculated at DFT levels, especially at B3LYB level, is due to the flat potential energy surface around TS. This phenomenon does not exist at MP2 and HF levels.

In order to analyze the change of the reaction dynamics in terms of the electronic structures, we monitored the spin densities of several atoms along the reaction pathway as shown in Fig. 4, and their values at several important points along the reaction pathway were also listed in Table 3. During the abstraction process, the spin density transfers from the $O_{radical}$ to the C_α starts around TS and the major transfer takes place around the abstraction point for all the calculation levels. There is a distinct pattern of spin density transfer between DFT and non-DFT methods in the way this spin density transfer takes place. For example, at the B3LYP level, the spin density of the hydroxyl oxygen transfers to the C_α changes slowly but does so rapidly when approaching the abstraction point. The major spin density transfer between the OH radical and the C_α happens at a very late stage in the reaction path. At the HF level, the spin density transfer between the $O_{radical}$ and the C_α arises at an early stage, and about 35% of the spin density of the OH radical has transferred to the C_α before reaching the TS compared to around 10% transfer at the TS at B3LYP level. After the abstraction point, the spin densities of all the species reach their plateau values rapidly at all the calculation levels. However, the amount of these spin density distributions among those atoms varies between these five methods. For HF and MP2 methods, almost all the $O_{radical}$ spin density transfers to the C_α but the C_α spin density is substantially less for the three DFT methods employed. At the DFT levels, the spin density of the nitrogen atom increases as the spin density of the C_α increases. This indicates that the spin density of the OH radical was transferred to the C_α and then transferred to the nitrogen atom from the C_α presumably through the captodative effect [24], which is one of the major factors to stabilize the abstraction product. At the MP2 and HF levels, however, only a slight increase in the spin density of the nitrogen atom was observed and this means that the

Table 4 The correlation between the spin density of C_α, energy barrier and local geometry

Level	$^a\Delta D$ (°)	^{b}Spin density of C_α	^{c}Ea (kcal/mol)	^{d}B(C_α-H_α)
B3LYP	1.5	0.081	0.8	1.117
M05-2X	5.4	0.194	3.5	1.155
BHandHLYP	6.2	0.252	5.8	1.177
MP2	6.3	0.331	7.5	1.180
HF	9.6	0.540	25.0	1.268

^{a} ΔD is the dihedral angle difference between reactant and TS

^{b} Spin density of C_α at TS taken from Table 3

^{c} Ea is TS barrier with ZPE taken from Table 2

^{d} B(C_α-H_α) is the ^{3}C-^{4}H bondlength taken from Table 1

captodative effect is not the major factor in stabilizing this carbon-centered radical in these two methods. Furthermore, there is a dip in the spin density of the H_α around the abstraction starting point at the MP2 and HF levels, but this dip was barely observed at the BHandHLYP level and not observed at the B3LYP and M05-2X levels. This phenomenon can be attributed to the TS abstraction mode. Since the abstraction is mainly through the bond stretching of the C_α-H_α bond at the HF and MP2 levels, the H_α plays some role in spin density transfer. While at the DFT levels the abstraction involves certain rocking motion and the H_α stays between the hydroxyl oxygen and the C_α only for a short period of time, and therefore plays a limited role in spin density transfer. The relationship between the geometry of the TS and its charge distribution are the main reasons for the above observations.

After the hydrogen abstraction, the C_α changes from sp^3 to sp^2 hybridization, corresponding to the geometry change from tetrahedron to triangular plane. This geometry change can be characterized by the dihedral angle (^{1}N-^{3}C-^{5}C-^{12}H) difference between the TS and reactant. We listed this difference at the five calculation levels in Table 4 along with related information to demonstrate the abstraction pattern. The smaller change in the dihedron angle indicates that the C_α retains more sp^3 characteristics and the TS is more reactant-like and therefore the barrier height is smaller. However, as the sp^2 characteristics of the C_α increases, the C_α spin density increases to push the H_α toward the OH radical to cause the increase in C_α-H_α length and the TS is more product-like and therefore the barrier height is larger. Therefore, the abstraction mode adopted by a particular calculation level just reflects the consequence of the amount of spin density transferred to the C_α and the way which the TS geometry was stabilized. However, the barrier height of the H_α abstraction in a given protein also depends on the electron-withdrawing ability for the side chain of a particular amino acid and the interaction between the residues in that protein, particularly the hydrogen bonding interaction. The former determines the amount of the spin density transferred to the C_α at the TS and the latter is crucial for the conformation of the peptides or proteins and then influences the stability of the TS geometry for either tetrahedron or triangular plane. Lu *et al.* [15] showed that the barrier height of the H_α abstraction strongly depends on the secondary structures. Generally, the barrier height increases with a high electron-withdrawing ability of the side chain and the interactions around the abstraction site destabilizing the tetrahedron geometry of the TS. Currently we are investigating this side chain effect of various amino acids and the influence of the secondary structure on for the OH H_α abstraction.

Conclusions

We successfully demonstrated the difference of reaction dynamics in the OH hydrogen abstraction from glycine between five different *ab initio* methods through the analyses of TS geometries, the TS vibration mode and spin density transfer. The later the H_α abstraction happens after TS, the smaller the barrier height. The barrier height underestimated at the B3LYP level is due to overemphasis on the rocking motion in the TS imaginary vibration mode. The overestimated barrier height at the HF level is due to overemphasis on the bond-stretching in the TS imaginary vibration mode. The actual TS vibration mode should be a mixture of these two motions in the proper combination, and this provides some physical ground for the scheme adopted by Song *et al.* [9] to improve the DFT results. The barrier height of the H_α abstraction can be determined not only by the calculation levels but also the local environment of the abstraction site. The captodative effect to stabilize the carbon-centered radical can only be observed in DFT levels but not in HF and MP2 levels. The hybrid DFT, BHandHLYP, can provide accurate results in this model system. We believe this study can shed some light in understanding the influence on the reaction dynamics using different calculation levels and provide a basis for the choice of *ab initio* method in protein oxidation.

References

1. Curtiss LA, Raghavachari K, Redfern PC, Pople JA (2000) J Chem Phys 112:7374–7383
2. Tuma C, Boese AD, Handy NC (1999) Phys Chem Chem Phys 1:3939–3947
3. Gonzalez L, Mo O, Yanez M (1997) J Comput Chem 18:1124–1135
4. Johnson BG, Gill PMW, Pople JA (1993) J Chem Phys 98:5612–5626
5. Toulouse J, Colonna F, Savin A (2004) Phys Rev A 70:62505
6. Zhao Y, Gonzalez-Garcia N, Truhlar DG (2005) J Phys Chem A 109:2012–2018
7. Johnson BG, Gonzales CA, Gill PMW, Pople JA (1994) Chem Phys Lett 221:100–108
8. Song JW, Tokura S, Sato T, Watson MA, Hirao K (2007) J Chem Phys 127:154109
9. Song JW, Hirosawa T, Tsuneda T, Hirao K (2007) J Chem Phys 126:154105
10. Goll E, Werner HJ, Stoll H, Leininger T, Gori-Giorgi P, Savin A (2006) Chem Phys 329:276–282
11. Leininger T, Stoll H, Werner HJ, Savin A (1997) Chem Phys Lett 275:151–160
12. Truhlar DG, Gordon MS (1990) Science 249:491–498
13. Truhlar DG, Steckler R, Gordon MS (1987) Chem Rev 87:217–236
14. Fukui K (1970) J Phys Chem 74:4161–4163

15. Lu H-F, Li F-Y, Lin S-H (2007) J Comput Chem 28:783–794
16. Cheng W-C, Soonmin J, Wu C-C, Lin R-J, Lu H-F, Li F-Y (2009) J Comput Chem 30:407–414
17. Himo F (2000) Chem Phys Lett 328:270–276
18. Yu D, Rauk A, Armstrong DA (1995) J Am Chem Soc 117:1789–1796
19. Csaszar AG, Perczel A (1999) Prog Biophys Mol Biol 71:243–309
20. Galano A, Alvarez-Idaboy JR, Montero LA, Vivier-Bunge A (2001) J Comput Chem 22:1138–1153
21. Zhao Y, Schultz Nathan E, Truhlar DG (2006) J Chem Theor Comput 2:364–382
22. Vincenzo B, Maurizio C (1997) J Chem Phys 107:3210–3221
23. Frisch MJ, Trucks GW, Schlegel HB, Scuseria GE, Robb MA, Cheeseman JR, Montgomery JA Jr, Vreven T, Kudin KN, Burant JC, Millam JM, Iyengar SS, Tomasi J, Barone V, Mennucci B, Cossi M, Scalmani G, Rega N, Petersson GA, Nakatsuji H, Hada M, Ehara M, Toyota K, Fukuda R, Hasegawa J, Ishida M, Nakajima T, Honda Y, Kitao O, Nakai H, Klene M, Li X, Knox JE, Hratchian HP, Cross JB, Bakken V, Adamo C, Jaramillo J, Gomperts R, Stratmann RE, Yazyev O, Austin AJ, Cammi R, Pomelli C, Ochterski JW, Ayala PY, Morokuma K, Voth GA, Salvador P, Dannenberg JJ, Zakrzewski VG, Dapprich S, Daniels AD, Strain MC, Farkas O, Malick DK, Rabuck AD, Raghavachari K, Foresman JB, Ortiz JV, Cui Q, Baboul AG, Clifford S, Cioslowski J, Stefanov BB, Liu G, Liashenko A, Piskorz P, Komaromi I, Martin RL, Fox DJ, Keith T, Al-Laham MA, Peng CY, Nanayakkara A, Challacombe M, Gill PMW, Johnson B, Chen W, Wong MW, Gonzalez C, Pople JA (2004) Gaussian. Gaussian Inc, Wallingford
24. Jonsson M, Wayner DDM, Armstrong DA, Yu D, Rauk A (1998) J Chem Soc. Perkin Trans 2(1998):1967–1972